Publ. Astron. Soc. Aust., 1998, 15, 132–5

HI Supergiant Shells in the Large Magellanic Cloud

S. Kim[1], L. Staveley-Smith[2], R. J. Sault[2], M. J. Kesteven[2], D. McConnell[2], M. A. Dopita[1] and M. Bessell[1]

[1]Mount Stromlo and Siding Spring Observatories, Weston Creek PO, ACT 2611, Australia
sek@mso.anu.edu.au
[2]Australia Telescope National Facility, CSIRO, PO Box 76, Epping, NSW 2121, Australia

Received 1997 August 1, accepted 1997 December 30

Abstract: The recently completed HI mosaic survey of the Large Magellanic Cloud (Kim et al. 1997) reveals complex structure in the interstellar medium, including filaments, arcs, holes and shells. We have catalogued giant and supergiant HI shells and searched for correlations with Hα emission, using a new image taken with a camera lens mounted on the 16-inch telescope at Siding Spring Observatory.

Keywords: galaxies: Large Magellanic Cloud — interstellar: HI, Hα — radio lines: atomic

1 Introduction

A rather complete review of recent work related to the Large Magellanic Cloud (LMC) has been given by Westerlund (1997). The overall distribution of the neutral hydrogen gas in the LMC and its relation to the SMC and the Galaxy had been described in the papers of McGee & Milton (1966), Rohlfs et al. (1984) and Luks & Rohlfs (1992). The neutral hydrogen (HI) gas in the LMC has been surveyed with the Australia Telescope Compact Array* (ATCA) at λ 21 cm. Compared to previous surveys of McGee & Milton (1966), Rohlfs et al. (1984) and Luks & Rohlfs (1992) using the Parkes telescope, the spatial resolution of the new survey is much higher: 1′ compared with 14′–15′. We compare the large-scale distribution of HI in the LMC with the result of a recent Hα survey, taken with a camera lens mounted on the 16-inch telescope at Siding Spring Observatory. The Hα images cover the same area as the HI mosaic survey, and have a spatial resolution of 20″, slightly better than the HI resolution. These two surveys combined offer a unique probe into the detailed relationship between the ionised and atomic phases in the interstellar medium of the LMC for the first time. The HI observations are summarised in Section 2, the Hα observations are summarised in Section 3 and results of correlations are given in Section 4.

2 HI Observations and Data Reduction

The LMC was observed using four configurations of the ATCA in: 1994 October 26–November 9 (750D); 1995 February 23–March 11 (750A); 1995 June 2–7 and 1995 October 15–31 (750B); and 1996 January 27–February 8 (750C). The combined configuration has 40 independent baselines ranging from 30 to 750 m, with a baseline increment of 15·3 m. This results in an angular resolution of 1.′0 for the data presented here. The largest-scale structure that the present image is sensitive to is ∼0.°6. The bandwidth used was 4 MHz, divided into 1024 channels (400 channels after the on-line application of Hanning smoothing and edge rejection). The observing band was centred on 1·419 GHz, corresponding to a central heliocentric velocity of 297 km s^{-1}, a velocity coverage of −33 to 627 km s^{-1}, and a velocity resolution of 1·65 km s^{-1}.

The LMC was divided into 12 regions, each containing 112 pointing centres. Each pointing centre was observed for 15 s, and good *uv* coverage was obtained by returning to each pointing centre approximately 29 times during the course of a typical observing day of 15 h. Each observation consisted of alternate scans of 28 min on the LMC and 3 min on the secondary (phase and amplitude) calibrator PKS B0407–658 or PKS B0454–810. The primary ATCA calibrator, PKS B1934–638 (assumed flux density 14·9 Jy at 1·419 GHz), was observed at the start of each observing day. These observations served both for bandpass calibration and flux density calibration.

The data were edited, calibrated and mosaiced in MIRIAD. The pixel size is 20″ and the size of the LMC cube is 1998×2230×120. The *uv* data were superuniformly weighted (Sramek & Schwab 1989) with an additional Gaussian taper, Fourier-transformed and mosaiced in the image plane. The maximum entropy method was used to deconvolve this cube. The final cube was constructed by convolving the maximum entropy model with a

* The Australia Telescope is funded by the Commonwealth of Australia for operation as a National Facility managed by CSIRO.

 1323-3580/98/010132$05.00

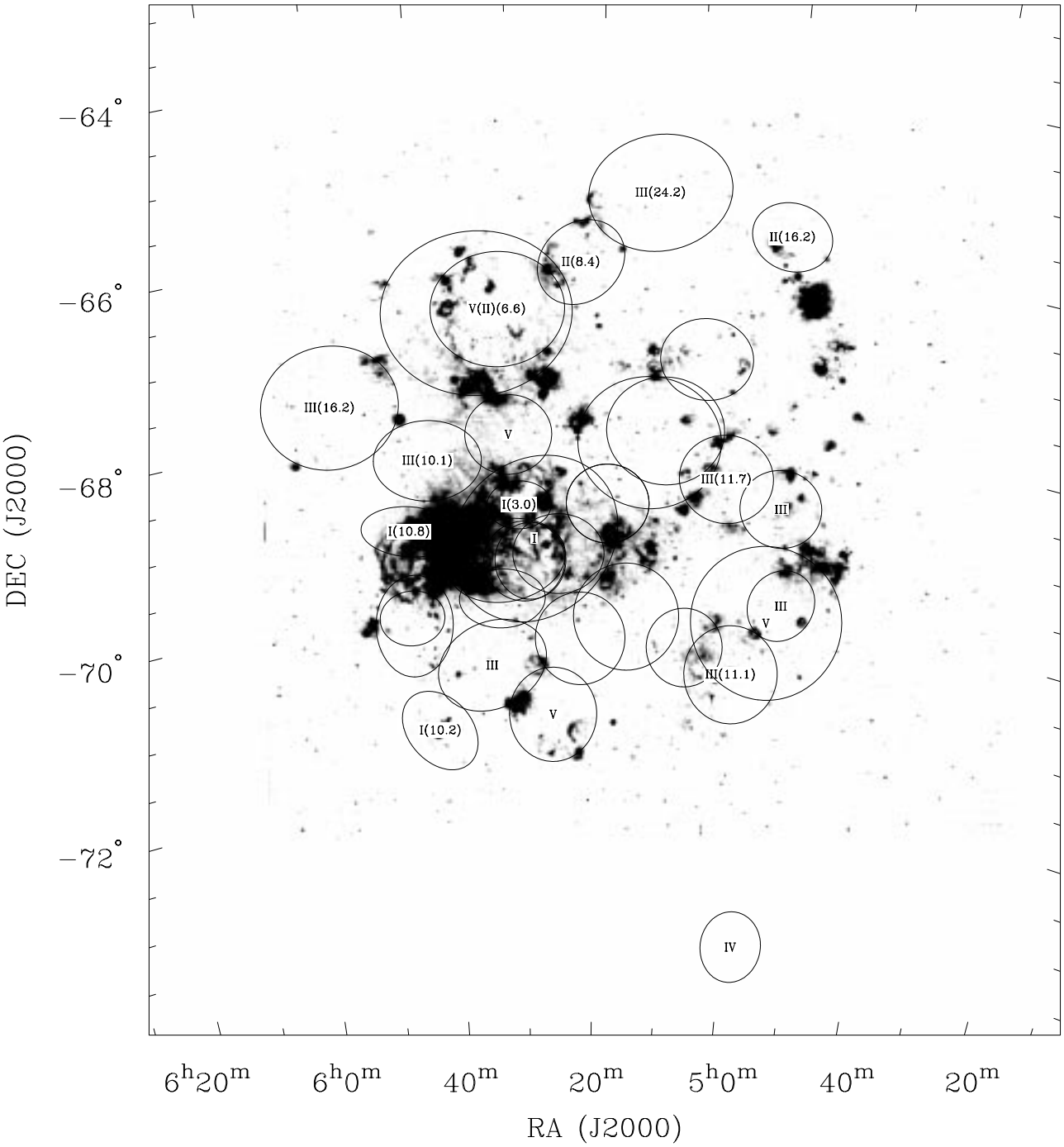

Figure 1—Positions of the candidate supergiant shells are overlayed as ellipses on the SSO Hα image. The classification, based on a comparision between the HI and Hα properties, is marked (see text). The numbers indicate the dynamical ages of the shells in Myr.

Gaussian of FWHM $1'\times1'$. The final rms noise, measured in line-free parts of the final cube, is 9 K.

3 Hα Observations and Data Reduction

For the wide-field survey of Hα emission in the LMC, a 153 mm $f/5{\cdot}0$ camera lens from the $2{\cdot}3$-m telescope at Siding Spring Observatory was mounted on the 16-inch telescope with a filter assembly and a cooled 2048 × 2048 CCD. Each 15 μm pixel corresponds to $20.''63$ on the sky, giving a total field size of $11{\cdot}7^\circ$ square. The Hα filter was centred at 6569 Å with a FWHM of 15 Å. Continuum subtraction was done with another image centred at 6620 Å. The exposure time for both Hα and continuum images was 4×900 s.

4 Results

The peak brightness temperature map (Kim et al. 1997) of the LMC shows many filamentary features, combined with HI holes and shells. In our preliminary

https://doi.org/10.1071/AS98132 Published online by Cambridge University Press

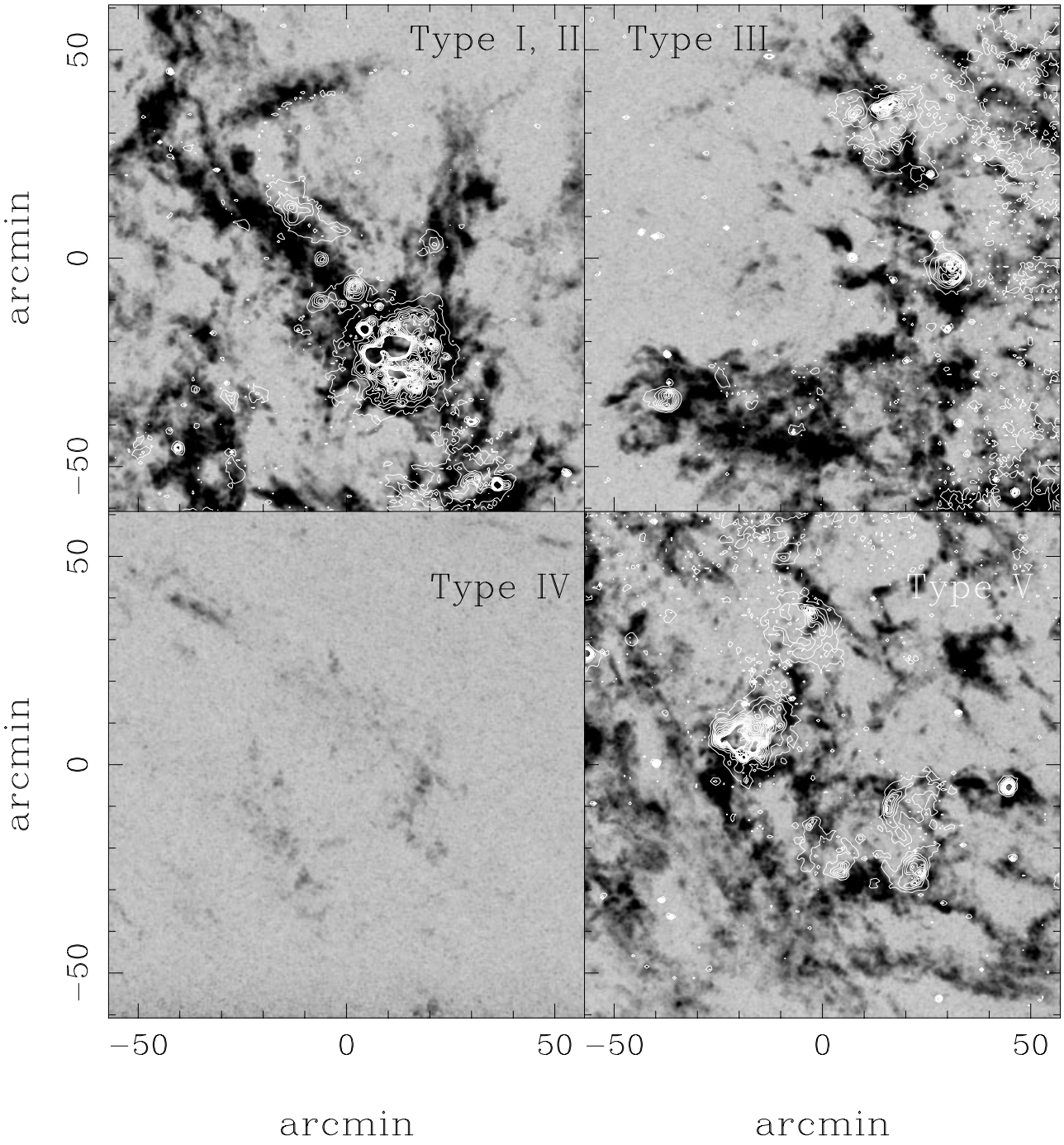

Figure 2—Geometrical relationship between HI (gray scale) and Hα (contours) for the five categories of HI shells described in the text.

analysis we have defined 32 HI supergiant shells; these shells are overlayed on the Hα image in Figure 1. The selection criteria applied to the shells are: (1) they must be edge-brightened ring-like structures larger than 600 pc that are visible in at least three integrated channel maps (the spacing between each integrated channel map is 5 km s^{-1}); and (2) the approaching and receding hemispheres (or one of the hemispheres) must be visible in position–velocity cuts (P–V diagrams).

Many of the shells are not simple expanding shells in the P–V diagrams. The cause of this is a combination of confusion between neighbouring shells, lack of zero-spacing data and breakouts from the disk of the LMC. If we compare the distribution of HI supergiant shells in each of the four quadrants of the LMC, we clearly see that the largest number of shells is located in the south-eastern quadrant, near the 30 Doradus nebula, as seen in Figure 1. Figure 1 also shows the age of each shell, t_s (in

https://doi.org/10.1071/AS98132 Published online by Cambridge University Press

units of Myr), calculated from $t_s = \frac{3}{5}R_s/V_s$ as given by the standard theory of wind-driven bubbles (Weaver et al. 1977), where R_s is the shell radius and V_s is the expansion velocity of the shell. The measured ages of the expanding supergiant shells are distributed between 3 and 25 Myr. The shells in Figure 1 may also be classified morphologically by comparing their HI and Hα structures. We define five categories for the geometrical correlation between HI and Hα emission (Figure 2). These categories should approximate an age sequence. In Type I shells, the HI shells are filled with ionised gas or else include discrete HII regions inside the HI shell. In Type II shells, the ionised gas forms a thin shell and has been trapped by the HI shell. Type III represents HI shells that have discrete HII regions on the wall of the shell. Type IV represents HI shells that are not associated with ionised gas. Type III and Type IV may both have evolved from Type II, with the difference between the two types probably dependent on the density of the interstellar medium. Type V are HI shells that have morphologically complex structure, which might be due to distortions caused by the secondary star formation on the surface of the shell. Age estimates for some of the shells marked in Figure 1 are due to uncertain or unmeasurable expansion velocities.

Kim, S., Staveley-Smith, L., Sault, R. J., McConnell, D., Kesteven, M. J., & Freeman, K. C. 1997, PASA, 14, 119
Luks, T., & Rohlfs, K. 1992, A&A, 263, 41
McGee, R. X., & Milton, J. A. 1966, Aust. J. Phys., 19, 343
Rohlfs, K., Kreitschmann, J., Siegman, B. C., & Feitzinger, J. V. 1984, A&A, 137, 343
Sramek, R. A., & Schwab, F. R. 1989, in Synthesis Imaging in Radio Astronomy, ed. R. A. Perley et al. (San Francisco: ASP), p. 123
Weaver, R., McCray, R., Castor, J., Shapiro, P., & Moore, R. 1977, ApJ, 218, 377
Westerlund, B. E. 1997, The Magellanic Clouds (Cambridge Univ. Press)

https://doi.org/10.1071/AS98132 Published online by Cambridge University Press